CHEMISTRY

Metal-free activation of molecular oxygen by covalent triazine frameworks for selective aerobic oxidation

Sara Abednatanzi[1]*, Parviz Gohari Derakhshandeh[1]*, Karen Leus[1], Henk Vrielinck[2], Freddy Callens[2], Johannes Schmidt[3], Aleksandr Savateev[4], Pascal Van Der Voort[1]†

Oxygen activation is a critical step in ubiquitous heterogeneous oxidative processes, most prominently in catalysis, electrolysis, and pharmaceutical applications. We present here our findings on metal-free O_2 activation on covalent triazine frameworks (CTFs) as an important class of N-rich materials. The O_2 activation process was studied for the formation of aldehydes, ketones and imines. A detailed mechanistic study of O_2 activation and the role of nitrogen heteroatoms were comprehensively investigated. The electron paramagnetic resonance (EPR) and control experiments provide strong evidence for the reaction mechanism proving the applicability of the CTFs to activate oxygen into superoxide species. This report highlights the importance of a self-templating procedure to introduce N functionalities for the development of metal-free catalytic materials. The presented findings reveal an important step toward the use of CTFs as inexpensive and high-performance alternatives to metal-based materials not only for catalysis but also for biorelated applications dealing with O_2 activation.

INTRODUCTION

One of the challenges for the future generations of chemists and environmental experts is to evolve catalytic processes that integrate environmental objectives into global industrialization (*1*). Most catalytic processes are commanded by the use of noble, transition, or rare-earth metals, acting as active sites (*2*–*4*). Among various catalytic processes, O_2 activation is at the heart of many potential applications, most importantly in fine chemical synthesis, and environmental remediation (*5*, *6*). A very promising area in bioinorganic chemistry lies in the field of metal-activated enzymes with transition-metal sites to activate molecular oxygen (*7*–*9*). In inorganic chemistry, Pt is the preferred metal for oxygen activation, although other metals such as Ir, Au, Cu, Ni, and Pd have revealed the capability of promoting the process as well (*10*, *11*). Despite the high efficiency, most metal-based catalytic systems suffer from low availability, high prices for the noble metals, deactivation of the catalyst, high cost for the purification, and disposal of products and waste (*11*). Therefore, the development of low-cost metal-free catalysts demonstrating comparable and even superior performance in comparison to the metal-based materials is highly desirable as alternatives to the present systems (*12*, *13*).

Nanocarbon materials such as carbon black (*14*), carbon nanotubes (*15*), graphene (*16*) or graphene oxide (*12*), and graphitic carbon nitride (*17*) have shown promising potential in various catalytic processes. Nevertheless, most of these materials without the presence of dopants are inactive in catalysis due to the weak interaction of reactants with carbon-based materials arising from the uniform charge distribution. The introduction of nonmetal heteroatoms (N, P, S, B, etc.) into the carbon matrix can modulate the electronic structure through charge delocalization that helps to achieve a high catalytic activity (*18*–*24*). Furthermore, new structural defects can be induced into the carbon backbone (*25*–*27*). Hence, an advanced modification of the pure carbon with heteroatom dopants as active sites can result in an enhanced performance. In 2013, Garcia and co-workers (*28*) demonstrated that N- and B-doped graphene materials are active metal-free catalysts to activate molecular O_2 in the aerobic oxidation of different substrates including benzylic compounds and cycloalkanes.

Covalent organic frameworks (COFs) are porous materials with robust carbon backbones (*29*, *30*). These COFs have exclusive features including high surface areas, excellent stabilities, adjustable pore size, and controllable chemical composition (*31*, *32*). Covalent triazine frameworks (CTFs) as unique COFs, reported in 2008 by Thomas and Antonietti (*33*), are created by linking light elements (C, O, and N). In general, CTFs can be classified into two categories, i.e., amorphous (*34*, *35*) and crystalline (*36*). These materials can offer a good opportunity to develop highly efficient heterogeneous metal-free (photo) catalysts in the future (*37*–*39*).

The key to overcome the limitations of metal-free systems and to study the O_2 activation mechanism in a controlled way lies in a precise control of the active sites, which can be obtained by reducing the carbonization degree of the materials. Accordingly, we introduce here a unique and previously unidentified potential application of CTFs as metal-free catalysts for environmentally friendly oxidation reactions. For this purpose, we used the cheap and easily available 1,4-dicyanobenzene (DCB) as the N-containing precursor to obtain CTF-1, via a simple self-templating procedure (*40*). The direct introduction of the dopant followed by the relatively low polymerization temperature (400°C) results in a better control over the structure of CTFs (*41*). Accordingly, materials with a homogeneous distribution of the heteroatom dopants can be obtained. This catalyst displayed an unprecedented performance in the oxidation reactions and can be considered as one of the best metal-free carbon-based catalysts ever reported.

[1]Center for Ordered Materials, Organometallics and Catalysis, Ghent University, Krijgslaan 281-S3, 9000 Gent, Belgium. [2]Department of Solid State Sciences, Ghent University, Krijgslaan 281-S1, B-9000 Ghent, Belgium. [3]Technische Universität Berlin, Institut für Chemie–Funktionsmaterialien, Hardenbergstraße 40, 10623 Berlin, Germany. [4]Max-Planck Institute of Colloids and Interfaces, Department of Colloid Chemistry, Research Campus Golm, 14424 Potsdam, Germany.
*These authors contributed equally to this work.
†Corresponding author. Email: pascal.vandervoort@ugent.be

RESULTS

Characterization of the CTFs synthesized at different temperatures

The CTF materials were synthesized following the procedure reported by Antonietti and co-workers (*40*), applying the typical ionothermal conditions as depicted in Fig. 1A. After the reaction, the $ZnCl_2$ is removed by extensive washing with water and then refluxing at 120°C in 1 M HCl [0.15 weight % (wt %) Zn remains analyzed by inductively coupled plasma]. To understand the specific role of dopants in the CTF materials, the polymerization temperature is increased from 400° to 600°C, and the obtained materials are labeled with the polymerization temperature (e.g., CTF-1-400).

Diffuse reflectance infrared Fourier transform spectroscopy (DRIFTS) and x-ray photoelectron spectroscopy (XPS) were performed to obtain more understanding of the structural characteristic of the nitrogen functionalities. In the DRIFT spectrum of CTF-1-400 (Fig. 1C), vibrational peaks appear at ~1360 and ~1550 cm^{-1}, demonstrating the presence of triazine fragments in the sample (*42*). The absence of the signal at ~2200 cm^{-1}, characteristic of the nitrile group, indicates the complete consumption of monomer and the formation of triazine linkages (*43*). The deconvolution of the N 1s XPS spectrum (Fig. 1D) results in a peak at 398.49 eV, indicating the presence of pyridinic nitrogen in the triazine rings. Furthermore, the N 1s XPS spectrum of CTF-1-400 shows three peaks at 400.16, 400.93, and 404.65 eV, representing the pyrrolic, quaternary, and oxidized N-O species (*44*). Besides the characterization of the species containing the nitrogen moieties, the porosity and pore structure of the CTF-1 material are important as well. As demonstrated in Fig. 1E, CTF-1-400 displayed a rapid N_2 uptake at low relative pressures, which is indicative of a highly microporous material (type I isotherm) (*45*). The CTF-1-400 exhibits a Brunauer-Emmett-Teller (BET) surface area of 1495 m^2g^{-1}, which was calculated in the linear range determined through the consistency criteria (*46*). The total pore volume is found to be 0.86 $cm^3\ g^{-1}$. The powder x-ray diffraction (XRD) pattern of the CTF-1-400 (Fig. 1F) exhibits a broad diffraction peak at $2\theta \sim 26°$ assigned to (001) reflection, indicating a "graphitic" layer stacking. Elemental mapping (Fig. 1G) further revealed a fine and homogeneous distribution of the elements, including N and C, from the CTF-1-400 material.

The DRIFT spectra of the CTFs-1 synthesized at higher temperatures (500° to 600°C) represent an overall reduction in the peak intensity, which is due to the further cross-linking/rearrangement reactions toward typical graphenal polymer structures as shown in Fig. 1B (*47*). The diffraction peak at $2\theta \sim 20°$ to 30° broadened and weakened with elevated trimerization temperature, which can be related to the structural rearrangements. The N_2 adsorption isotherms change from type I to type IV for CTFs-1 synthesized at higher temperatures, which indicates the formation of mesopores (Fig. 1E). In addition, the BET surface area tends to increase from 1495 to 2160 m^2/g when the polymerization temperatures are varied from 400° to 600°C (table S1). Raman spectroscopy was applied to identify the electronic structure of the CTFs (Fig. 1H). The observed two characteristic bands located around 1370 and 1607 cm^{-1} correspond to the D and G bands, which reveal the existence of lattice defects and porous two-dimensional honeycomb structure (*43*). It is important to note that the long-range order for the CTFs decreases with increasing polymerization temperature, which can be confirmed by the relative intensity of two peaks (I_D/I_G). The I_D/I_G ratio raised from 0.88 to 0.91 when the synthesis temperature was enhanced from 400° to 600°C.

Catalytic performance of the CTFs-1 for the selective aerobic oxidation of alcohols

It is well known that various carbon materials [N-doped activated carbon (*48*), P-doped graphitic carbon (*49*), and N-doped graphene (*50*)] have the potential to be used as metal-free catalysts in the aerobic oxidation of alcohols. However, these catalysts often exhibit fundamental drawbacks such as low efficiency (conversion <20%) or high catalyst loadings (200 wt %), as well as problems with catalyst recovery. Although the active sites and the mechanisms have not yet been completely understood, quaternary N atoms were found to be responsible for aerobic oxidation reactions (*48*). Within this context, our initial studies focused on the catalytic efficiency of CTFs-1 synthesized under both mild and ionothermal conditions. Therefore, crystalline CTF-1 (CTF-HUST-1) with a well-defined structure was synthesized via the low-temperature polycondensation reaction of 1,4-phthalaldehyde and terephthalamidine dihydrochloride following the method reported in the literature (*51*). The catalytic efficiency of CTF-HUST-1 without the presence of quaternary N atoms in the framework was compared with CTF-1-400 under the same reaction conditions. While 87% conversion of benzyl alcohol was observed using the CTF-1-400 catalyst (Table 1), the CTF-HUST-1 resulted in a remarkably lower conversion (5%) (Table 2, entry 1). This observation is an evidence for the essential role of the N functionalities for the development of efficient metal-free catalytic materials.

Further catalytic studies were performed on CTF-1-400 catalyst with intrinsic N-doping and controllable porous structures in the oxidation of a variety of primary and secondary alcohols (Table 1). We observed that the CTF-1-400 catalyst can catalyze the conversion of primary benzylic alcohols (~32 to 87%) within a short reaction time of 3 hours, but not secondary alcohols, which is consistent with the higher reactivity of the primary benzylic alcohols. It is important to note that the products of overoxidation (benzoic acid derivatives) were not detected even if the reaction was extended to longer reaction times, demonstrating the high selectivity of the CTF-1 catalyst toward aldehydes and ketones. We found that the conversion of unsubstituted benzyl alcohol is higher compared with the substituted substrates. This observation might be explained by the planar structure of benzyl alcohol, and therefore, the interaction between the catalyst's surface and the substrate is more efficient. Compared to aromatic alcohols, aliphatic/allylic alcohol substrates react more sluggishly and display very low conversions (3 to 7%). This reaction highly depends on the type of the applied base. When Cs_2CO_3 was replaced by other carbonates such as K_2CO_3 and Na_2CO_3, the conversions of benzyl alcohol were 23 and 10%, respectively, after 4 hours of reaction. In the absence of Cs_2CO_3 as the base, only a conversion of 8% was obtained. These results indicate that Cs_2CO_3 plays an important role to increase the catalytic activity in the aerobic oxidation of alcohols. In addition, with reducing the catalyst amount from 17 to 8.5 mg, still a high conversion of 61% was obtained after 0.75 hour. The turnover frequency (TOF) of the CTF-1-400 catalyst was 10 $hour^{-1}$ using benzyl alcohol as the substrate and 8.5 mg of the catalyst and was calculated as a ratio of the (millimoles of product)/(millimoles of quaternary N) per time (the role of quaternary N will be discussed in the mechanistic studies). Note that the catalytic efficiency of the CTF-1-400 catalyst both in terms of conversion and TOF was much higher compared with the reported metal-free catalysts for the aerobic oxidation of benzyl alcohol as depicted in Fig. 2 (*48*, *50*). Since the catalytic reactions in reports are

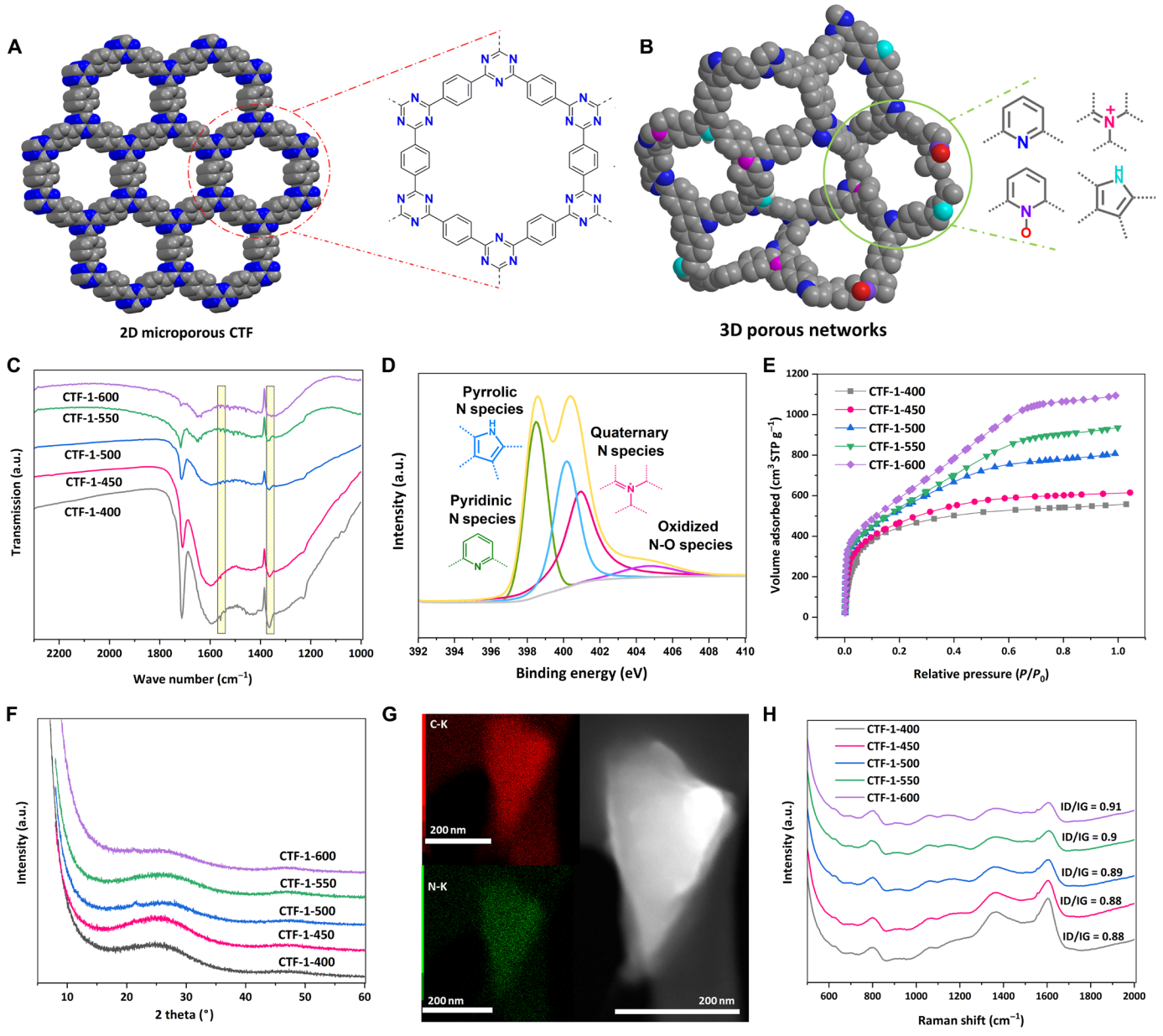

Fig. 1. Synthesis and structural characterization of CTFs synthesized at different temperatures. (**A**) Illustration of the ideal ordered structure of CTF-1. (**B**) Schematic representation of the possible structure at relatively high temperatures of synthesis (the ratios of nitrogen species of CTFs can be tuned through adjusting the reaction temperature). (**C**) DRIFT spectra. (**D**) N 1s XPS spectrum of the CTF-1-400. (**E**) Nitrogen adsorption isotherms. (**F**) Powder XRD patterns. (**G**) TEM image and elemental mapping images of CTF-1-400. (**H**) Raman spectra. a.u., arbitrary units.

done under different reactions conditions, N-doped activated carbon was synthesized according to the literature method (*52*). The catalytic activity of the obtained N-doped activated carbon was investigated under identical conditions as the CTF-1-400, resulting in only 10% conversion of benzyl alcohol after a 2 hours reaction. These observations indicate that the high catalytic performance of the CTF-1-400 catalyst can be ascribed to the higher content of N species compared with N-doped activated carbon and N-doped graphene nanosheets. In addition, the fabrication strategy using heteroatom-containing precursors at relatively low polymerization temperature may play an important role in the activity of the final porous material in metal-free catalysis. Compared with N-doped carbon materials that demand multiple postprocessing procedures to fabricate heteroatom-containing carbon-based catalysts, CTFs are generated by the direct use of heteroatom-containing linkers through simple self-templating procedures (*41*). While dislocation and/or inaccessibility of quaternary N atoms and lower catalytic activity can be expected in the N-doped carbon materials, CTFs provide materials with a homogeneous distribution of the heteroatom dopants. To investigate the catalytic potential of Zn as active sites in the oxidation reaction, an additional experiment was performed using homogeneous $ZnCl_2$ catalyst (0.02 mmol), and no product was produced after reaction at 100°C. From an environmental point of view, the catalytic reaction was also performed under solvent-free conditions

Table 1. Results of aerobic oxidation of several alcohols using the CTF-1-400 catalyst. Reaction conditions: 17 mg of CTF-1-400 catalyst, 0.33 mmol of substrate, 0.2 mmol of Cs2CO3, 330 μl of toluene, O2 (1 atm), 100°C, 3 hours for 2a–2i and 2p–2r, 12 hours for 2j–2o and 2s–2u. Conversions are an average of at least three runs. Full conversion (99%) was obtained for 2a to 2h after 12 hours. All substrates displayed >99% selectivity toward the corresponding aldehyde/ketone.

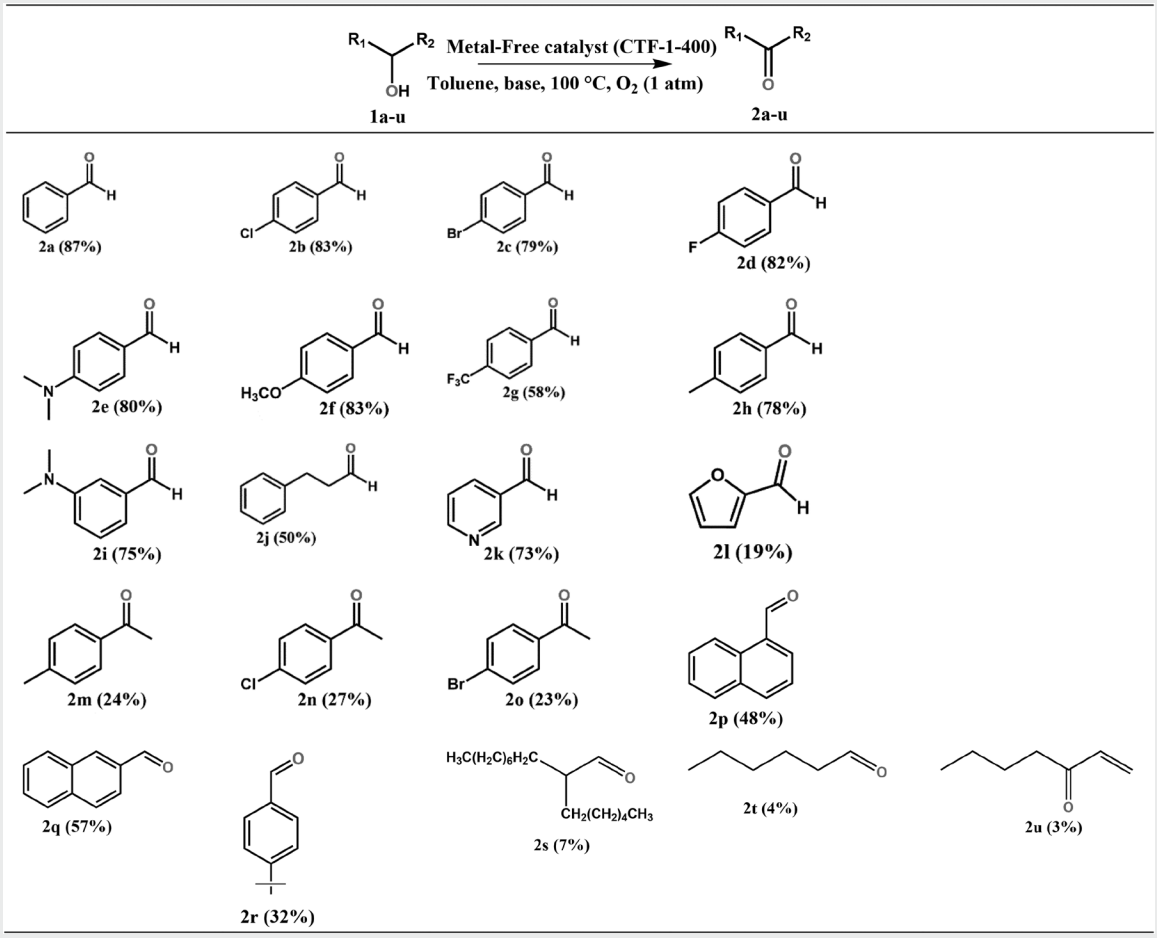

using 10 times more amount of benzyl alcohol and 17 mg of the catalyst. A good conversion of 35% was observed after 2 hours of reaction with a TOF of 10.8.

The wide applicability of CTFs for metal-free catalysis was further investigated using CTFs containing different monomers (2,6-dicyanopyridine and 4,4′-dicyanobiphenyl). The obtained materials were applied in metal-free catalysis for benzyl alcohol oxidation, which resulted in 99 and 60% conversions, respectively. A summary of the obtained data is shown in table S2. Among these monomers, DCB is preferred as the cheap and easily available N-containing precursor.

Catalytic performance of CTFs-1 for aerobic oxidative coupling of amines

Inspired by the great activity of the CTF-1 catalyst in the aerobic oxidation of alcohols, we proceeded to examine the broad application of this catalyst for another metal-free oxidation reaction. For this purpose, the CTF-1 catalyst was used in the oxidative coupling of amines to imines, which often proceeds via the initial generation of a superoxide radical anion ($^{\bullet}O_2^-$). At a low temperature (60°C) and a low atmospheric pressure of O_2 (1 atm), all substrates showed great conversion (99%) and high selectivity (>85%) for the formation of the related imines (table S3). A very low conversion of 4% was observed in the absence of the catalyst using benzylamine as the substrate under the applied reaction conditions.

Recyclability studies of CTF-1-400 catalyst

A major challenge in the development of metal-free catalysts is their recyclability. So far, some carbon-based metal-free catalysts have shown poor reusability due to the loss of their active sites or deactivation (*48*). The recyclability of the CTF-1-400 catalyst was examined in consecutive runs. The results demonstrated that CTF-1-400 could retain almost its full catalytic efficiency after four reaction cycles without a substantial loss of activity and selectivity (fig. S1A). No apparent change in the XPS spectrum of the recycled catalyst was observed. Furthermore, the recovered catalyst showed no notable

Table 2. Various control experiments to obtain insights into the reaction mechanism. Reaction conditions: 17 mg of catalyst, 0.33 mmol of benzyl alcohol, 0.2 mmol of Cs_2CO_3, 330 μl of toluene, O_2, 100°C, 2 hours for entries 2 to 7 and 12 hours for entries 1 and 8 to 16, Conversions are an average of at least three runs. n.d., not detected.

Entry	Catalyst	Conversion (%)	Selectivity (%)*
1	CTF-HUST-1	5	>99
2	CTF-1-300	35	>99
3	CTF-1-400	64	>99
4	CTF-1-450	69	>99
5	CTF-1-500	74	>99
6	CTF-1-550	87	>99
7	CTF-1-600	97	>99
8	No catalyst	<1	n.d.
9	CTF-1-400	99	>99
10†	CTF-1-400	3	>99
11‡	CTF-1-400	11	>99
12§	CTF-1-400	99	>99
13‖	CTF-1-400	99	>99
14¶	CTF-1-400	99	>99
15#	CTF-1-400	26	>99
16**	CTF-1-400	7	>99

*Selectivity toward benzaldehyde. †Under Ar atmosphere. ‡With *p*-benzoquinone as the superoxide ($^{\bullet}O_2^-$) scavenger. §With *tert*-butyl alcohol as the $^{\bullet}OH$ scavenger. ‖With NaN_3 as the $^1O_2$ scavenger. ¶With 1,3-diphenylisobenzofuran as the $^1O_2$ scavenger. #With ammonium oxalate. **The reaction was done at room temperature.

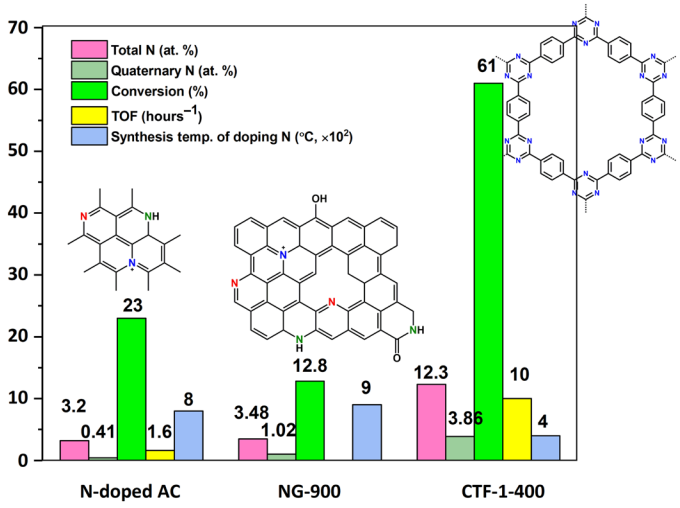

Fig. 2. Catalytic performance of CTF-1-400. Comparison of the CTF-1-400 catalyst with other N-doped carbon-based metal-free catalysts for aerobic oxidation of benzyl alcohol (*48*, *50*). Reaction conditions for CTF-1-400: 8.5 mg of CTF-1-400 catalyst, 0.33 mmol of substrate, 0.2 mmol of Cs_2CO_3, 330 μl of toluene, O_2 (1 atm), 100°C, 0.75 hour. AC, activated carbon.

reduction in the quaternary-type N species as was confirmed by XPS analysis (fig. S1B and table S4).

Mechanistic proposal for the oxidative process over CTFs-1

One of the main challenges in the development of N-doped carbon-based catalysts is the insufficient understanding of the exact active sites within the catalysts, which limits the control over their activity and selectivity. Within this context, we applied CTFs-1 synthesized at different temperatures to develop knowledge into the nature of the active sites. In addition, one more sample was prepared by lowering the reaction temperature to 300°C (CTF-1-300). The low reaction temperature mainly prevents initial carbonization and therefore results in a C/N weight ratio similar to the theoretical value of 3.43. As can be observed from Fig. 3A and table S5, the C/N ratio of the CTFs-1 increases notably as a function of increasing synthesis temperature. This observation confirms a reduction in the nitrogen content with an increase in the synthesis temperature because of the partial carbonization of the framework (*40*, *53*). Similar to the CTF-1-400 material, the XPS characterization of the samples synthesized at higher temperatures displays the existence of four different types of nitrogen functionalities including still pyridinic nitrogen in the triazine rings (398.4 eV), as well as pyrrolic (400 eV), quaternary (401 eV), and oxidized N-O (404 eV) species (Fig. 3, B to F). The conversion of benzyl alcohol enhanced, while the polymerization temperature is increased from 300° to 600°C (Table 2, entries 2 to 7). More specifically, almost full conversion (97%) was observed in the presence of CTF-1-600 after only 2 hours of reaction compared with 35% in the case of CTF-1-300. In addition, the calculated turnover numbers were 1.8, 3.9, 4.2, 4.4, 5.5, and 6 for CTF-1-300 to CTF-1-600 catalysts, respectively, and were obtained as a ratio of the (millimoles of product)/(millimoles of quaternary N). The conversion of benzyl alcohol is graphed against the number of nitrogen functionalities based on XPS analyses. The ratio of a nitrogen functionality in a CTF-1 sample is calculated concerning the total amount of N (Fig. 4A and table S6). The obtained conversions cannot be associated with the amount of pyridinic, pyrrolic, or oxidized nitrogen species; however, a good correspondence with the amount of quaternary-type N species is presented, confirming the crucial role of these N functionalities for proceeding the catalytic reaction. It is important to note that even CTFs-1 synthesized at the polymerization temperatures as low as 300° and 400°C still present the highest activity yet reported for this aerobic transformation (with regard to conversion and reaction time using metal-free N-doped carbon-based catalysts).

To achieve a mechanistic understanding of the aerobic oxidation reaction, a set of control experiments was performed. From the results summarized in Table 2, we observed that no product was produced in the absence of the catalyst (Table 2, entry 8). Furthermore, the conversion of benzyl alcohol toward benzaldehyde lowered to 3% under the Ar atmosphere, proving the crucial function of oxygen as the oxidant and confirming that oxygen species present in the structure of CTFs-1 are not involved in the oxidation reaction (entry 10 in Table 2). The addition of *p*-benzoquinone as the superoxide ($^{\bullet}O_2^-$) scavenger (*54*) into the reaction system containing CTF-1-400 as the catalyst suppressed the oxidation of benzyl alcohol (conversion 11%; Table 2, entry 11 versus 9). This observation indicates the unique applicability of CTFs to activate molecular oxygen to superoxide, which acts as oxidant species in the catalytic cycle. To elucidate whether other activated oxygen species are created in our system, different scavengers including *tert*-butyl alcohol

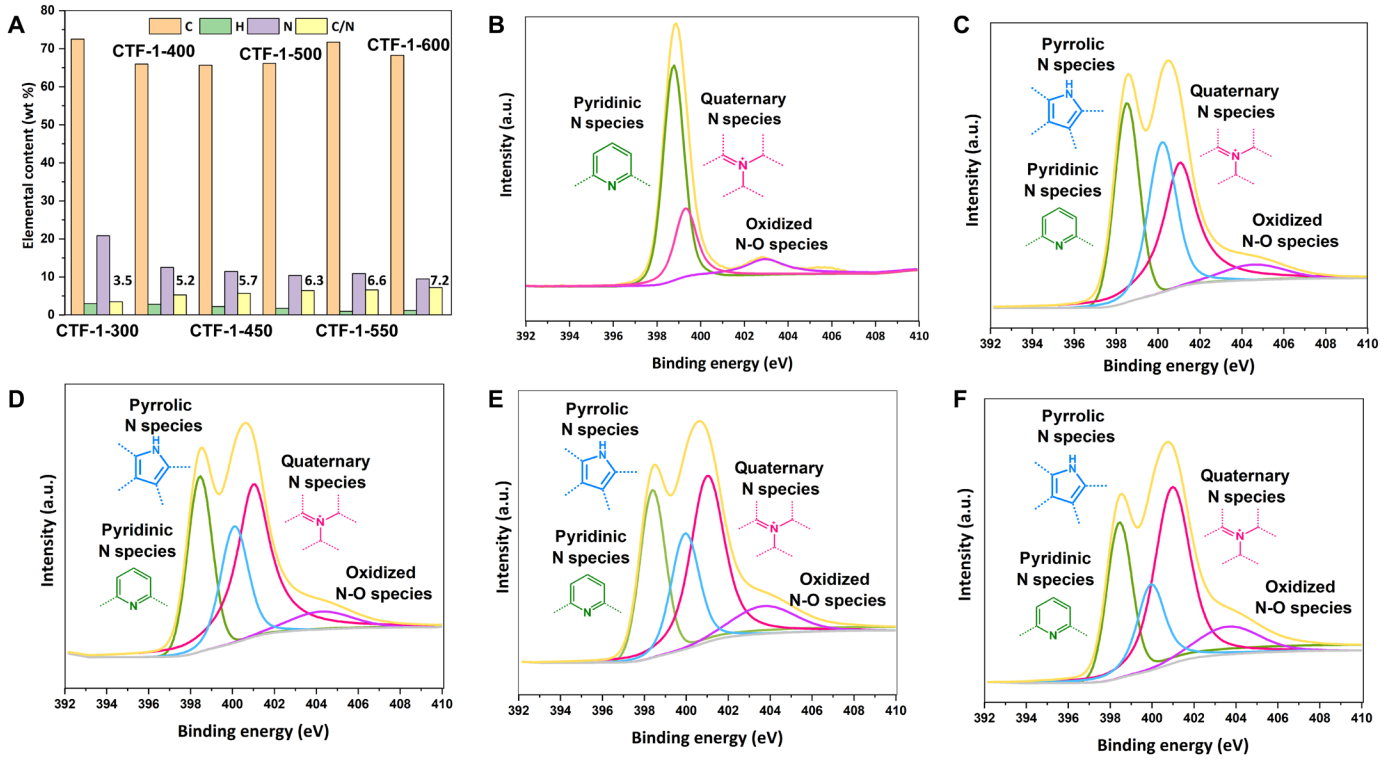

Fig. 3. Structural characterization of CTFs-1 synthesized at different temperatures. (**A**) Ratios of C/N determined by elemental analyses. (**B**) N 1s XPS spectrum of the CTF-1-300. (**C**) N 1s XPS spectrum of the CTF-1-450. (**D**) N 1s XPS spectrum of the CTF-1-500. (**E**) N 1s XPS spectrum of the CTF-1-550. (**F**) N 1s XPS spectrum of the CTF-1-600.

and NaN_3 were added into the reaction mixture to particularly hinder the formation of $^{\bullet}OH$ and $^1O_2$, respectively (*54*). In both cases, no reduction in the catalytic activities was observed (entries 12 and 13 in Table 2). Besides the use of NaN_3 as the common selective $^1O_2$ scavenger, 1,3-diphenylisobenzofuran was applied as another selective $^1O_2$ scavenger (*55*) with high solubility in the reaction media. No decrease in the catalyst activity was observed (Table 2, entry 14). Another control experiment was conducted using ammonium oxalate. Upon the addition of ammonium oxalate, the conversion of benzyl alcohol was inhibited to 26%, suggesting that oxidation of alcohol does not proceed in the presence of ammonium oxalate (Table 2, entry 15). In addition, lowering the reaction temperature from 100° to 25°C resulted in only 7% conversion of benzyl alcohol after 12 hours (Table 2, entry 16).

To obtain a profound understanding of the function of the CTF-1 material in oxygen activation, the mechanistic studies described above were complemented by electron paramagnetic resonance (EPR) analyses. To identify the generated active oxygen species in our catalytic system, 5,5-dimethyl-1-pyrroline N-oxide (DMPO), as the spin trapping agent, was added to the catalytic reaction mixture. As shown in fig. S2A, there is only a very weak EPR signal in the absence of the CTF-1 catalyst. For the reaction mixture containing CTF-1, a clear change of the EPR signals is revealed.

The EPR spectrum of the reaction mixture that contains CTF-1-400 shows a strong peak at $g = 2.0029 \pm 0.0002$, with a Lorentzian line shape and a peak-to-peak width of 0.27 mT (Fig. 4B). By a numerical elimination of the CTF-1 singlet, a sextet spectrum, in which each line shows an additional small splitting, can be quite successfully isolated (Fig. 4C, top trace, and fig. S2B). The latter spectrum can be convincingly assigned to an alkoxyl DMPO adduct. A spectrum simulation using the spin Hamiltonian parameters published by Buettner (*56*) for this type of adduct in a toluene solvent, as is the case here, exhibits a notable agreement with the experiment [$g = 2.0061$; $a_N = 1.284$ mT (^{14}N), $A_{H1} = 0.648$ mT (^{1}H), $A_{H2} = 0.168$ mT (^{1}H), Lorentzian peak-to-peak linewidth = 0.27 mT]. By replacing Cs_2CO_3 with Na_2CO_3 as base, the overall intensity of the EPR spectrum reduced notably (Fig. 4C). Similarly, the EPR spectrum of the reaction mixture in the absence of Cs_2CO_3 shows a very weak signal. According to the obtained data from EPR measurements and the performed control experiments, we assume that Cs_2CO_3 may facilitate the generation of the alkoxy intermediate in the catalytic cycle. A similar observation has been reported on a $[RuCl_2(p\text{-cymene})]_2/Cs_2CO_3$ catalytic system showing the efficiency of Cs_2CO_3 to generate an alkoxy ruthenium intermediate (*57*).

As a side product, H_2O_2 could be determined by the ultraviolet (UV)–visible absorption monitoring of potassium titanium(IV) oxalate in the reaction mixture, following the standard procedure described in the literature (fig. S2, C to E) (*58*).

With regard to the observed results from the control experiments and EPR measurements, we present a reaction pathway, as depicted in Fig. 4D. So far, many experimental and theoretical investigations have shown the applicability of N-doped carbon-based materials for adsorption and activation of molecular O_2 (*6*, *59*–*62*). Within this context, Arai and co-workers (*48*) proposed the adsorption of molecular oxygen on a carbon atom neighboring the quaternary N atom and/or on the carbon and nitrogen atoms, which results in the formation of some oxygen radicals. On the basis of our observations, we deduce that oxygen activation proceeds with the assist

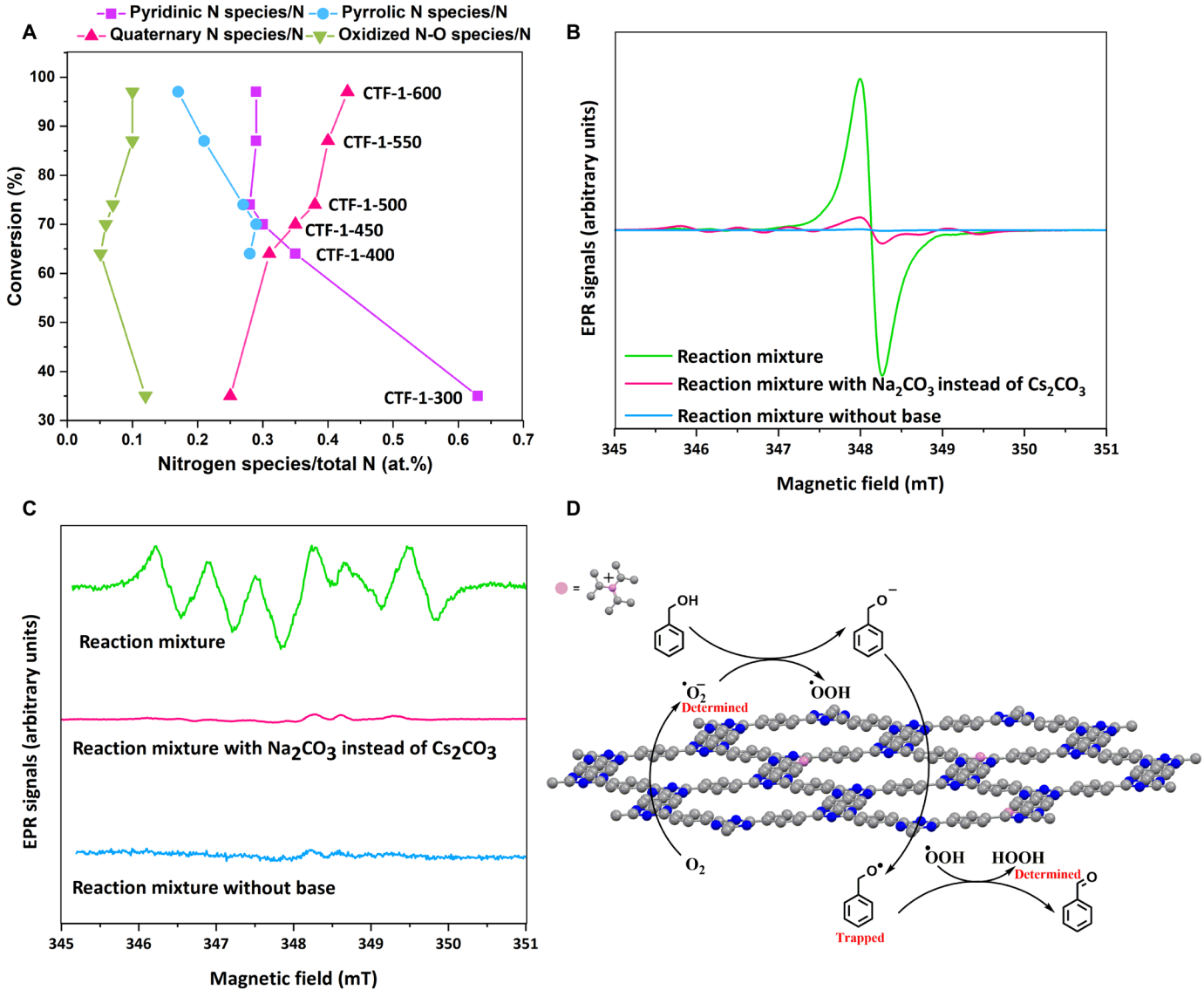

Fig. 4. Mechanistic studies. (**A**) Relationship between the conversion of benzyl alcohol and different N species within the CTF-1 materials synthesized at different temperatures [reaction conditions: 17 mg of catalyst, 0.33 mmol of substrate, 0.2 mmol of Cs_2CO_3, 330 μl of toluene, O_2 (1 atm), 100°C, 2 hours]. (**B**) Effect of base on the EPR spectra of CTF-1-400 in the reaction mixture. (**C**) For clarification, the EPR spectrum of the CTF-1-400 without DMPO is eliminated from that of the solution containing both the CTF-1 and the spin trap (DMPO). (**D**) Schematic representation of the proposed reaction mechanism for the oxidation of benzyl alcohol using CTF-1-400 as the metal-free catalyst.

of the quaternary N species of the CTF-1 material. We propose that the generated superoxide on the surface of CTF-1 reacts with benzyl alcohol and extracts one proton to generate $PhCH_2O^-$ by producing $^{\bullet}OOH$ moieties. Initially, the generated $PhCH_2O^-$ is oxidized into $PhCH_2O^{\bullet}$, which is consequently oxidized by $^{\bullet}OOH$ into benzaldehyde as the desired product.

To investigate whether the CTF-1-400 material is a radical initiator or a heterogeneous catalyst, a control experiment was performed using 17 mg of the CTF-1-400 catalyst. Accordingly, the catalyst was removed after a 0.5 hour reaction, and the catalytic reaction was continued for a further 2.5 hours, resulting in 35% conversion of benzyl alcohol. This result is the same as the obtained conversion after the 0.5 hour reaction, proving that the catalytic reaction stops in the absence of the catalyst.

Moreover, we conducted a set of control experiments (table S7) to find out the reaction pathway in the aerobic oxidative coupling of amines. On the basis of our observations and reported mechanistic studies (*63*, *64*), a possible mechanism is demonstrated in fig. S3.

DISCUSSION

In summary, we reveal the applicability of CTF-1 materials to activate O_2 at atmospheric pressure under mild conditions exemplified in the selective aerobic oxidation reactions. Our research successfully harnessed the power of CTFs-1 in O_2 activation for dehydrogenation and C—N bond generation reactions using molecular oxygen as the green oxidant. The reported findings highlight the importance of the self-templating procedure to introduce a large number of N

functionalities using low polymerization temperatures for the development of metal-free catalytic materials. Different synthesis temperatures to control the amount of dopant and the structural configuration within nanostructured frameworks were overviewed and discussed. The CTF-1 materials performed a great reusability, which is a long-standing challenge in many catalytic systems. We believe that the presented findings reveal an important step toward using CTFs not only as highly efficient metal-free catalysts for many important sustainable transformations but also as promising materials for biorelated applications dealing with O_2 activation.

MATERIALS AND METHODS

Catalyst preparation

Synthesis of CTF catalysts

The preparation of the CTF material was achieved according to the standard method reported in the literature (*40*) applying the typical ionothermal conditions. In general, a glass ampule was filled with DCB (213 mg, 1.66 mmol) and $ZnCl_2$ (1133 mg, 8.31 mmol) in a glovebox. The ampule was sealed under vacuum and placed in an oven at 300° to 600°C for 48 hours with a heating rate of 60°C/hour. After cooling to room temperature (RT), the ampule was opened, and the black-colored solid was stirred for 3 hours in 150 ml of H_2O, filtered, and washed with 150 ml of H_2O and 75 ml of acetone. The solid was refluxed at 120°C in HCl (1 M, 150 ml) overnight, filtered, and subsequently washed with HCl (1 M), H_2O, tetrahydrofuran (THF), and acetone. The powder was dried under vacuum overnight at 120°C. Crystalline CTF-1 (CTF-HUST-1) was synthesized via a low-temperature polycondensation reaction following the procedure presented in the report (*51*).

Catalytic reactions

The oxidation of alcohols was conducted in a Schlenk tube. During a catalytic test, the CTF catalyst (17 mg), base (0.2 mmol), dodecane (37.5 μl, 0.165 mmol), alcohol (0.33 mmol), and toluene (330 μl) were placed in the tube. The tube was purged with pure oxygen, sealed, and heated to 100°C for 2 to 12 hours. After each catalytic test, the catalyst was recycled through filtration, followed by washing with toluene and water to remove the excess amount of base. The catalyst was applied in the following runs.

The control tests using scavengers were done in a Schlenk tube. To a mixture of CTF-1-400 catalyst (17 mg), Cs_2CO_3 (65 mg, 0.2 mmol), and benzyl alcohol (34.3 μl, 0.33 mmol) in toluene (330 μl), the desired scavenger (0.33 mmol) was introduced. The catalytic reaction was done at 100°C for 12 hours. The control experiment using homogeneous $ZnCl_2$ catalyst was done as follows: A solution of catalyst (0.02 mmol), Cs_2CO_3 (65 mg, 0.2 mmol), and benzyl alcohol (34.3 μl, 0.33 mmol) in toluene (330 μl) was placed in the Schlenk tube. The tube was purged with pure oxygen, followed by sealing and heating to 100°C for 12 hours. Samples were withdrawn and were analyzed using a gas chromatograph [ultrafast equipped with a flame ionization detector (FID)].

For the purposes of H_2O_2 determination, 300 μl of the reaction mixture after centrifugation was transferred into a 2-ml volumetric flask. Then, the titanium reagent (1 ml), prepared following the standard procedure described in the literature (*58*), was added to the same volumetric flask, and the flask was filled with deionized water to a total volume of 2 ml. The UV-visible spectrum was recorded in the range of 200 to 800 nm. For the blank solutions, absorption from the titanium reagent (1 ml in a 2-ml volumetric flask and filled with deionized water) was recorded. Another control measurement was done for the possible colored organic compounds present in the reaction mixture. Three hundred microliters of the reaction mixture after centrifugation was transferred into a 2-ml volumetric flask and filled with deionized water to a total volume of 2 ml without the addition of the titanium reagent.

The aerobic oxidative coupling of amines was done in a Schlenk tube. During a general catalytic experiment, the CTF-1-400 catalyst (17 mg), dodecane (37.5 μl, 0.165 mmol), amines (0.33 mmol), and toluene (330 μl) were placed in the Schlenk tube. The tube was purged with pure oxygen, followed by sealing and heating to 60°C for 12 hours.

For control tests using scavengers, to a mixture of CTF-1-400 catalyst (17 mg) and benzylamine (0.33 mmol) in toluene (330 μl), the desired scavenger (0.33 mmol) was added. The catalytic reaction was done at 60°C for 3 hours. Samples were withdrawn and were analyzed using a gas chromatograph.

Materials and instrumentation

All reagents were obtained from Sigma-Aldrich or TCI Europe and applied as received. The CTF materials were characterized by x-ray powder diffraction (XRPD), N_2 adsorption, and scanning transmission electron microscopy (STEM) applying the instruments mentioned in our previous reports (*65*, *66*). XRPD measurements were carried out on an x-ray diffractometer (Thermo Fisher Scientific ARL X'Tra), performed at 40 kV, 40 mA, using Cu─Kα radiation (λ = 1.5406 Å). The porosity analysis was performed applying a BELSORP-mini II gas analyzer. The samples were activated at 120°C under vacuum before analysis. The catalytic activity of catalysts was monitored by gas chromatography (GC) having an FID. The ultrafast GC was equipped with a 5% diphenyl/95% polydimethylsiloxane column (10-m length and 0.10-mm internal diameter). Helium was used as the carrier gas and with 0.8 ml/min flow rate. GC–mass spectrometry (MS) analysis was conducted using an Agilent 6890 GC with a DB-5ms column, coupled with an Agilent 5973 MS using an electron ionization detector. Helium was used as the carrier gas with a constant flow of 2 ml/min. STEM images were collected applying a JEOL JEM-2200FS instrument with an accelerating voltage of 200 kV. Isopropanol was used to disperse the samples followed by ultrasonic irradiation for 10 min. A copper support TEM grid was immersed in the mixture and dried before imaging. The XPS measurements were done on a K-alpha Thermo Fisher Scientific spectrometer with a monochromatic Al Kα x-ray source. The EPR spectra were recorded with a Varian E-line spectrometer equipped with an HP 5342A microwave frequency counter. The magnetic fields were calibrated using the spectrum of diphenyl picryl hydrazyl (g = 2.0036). The spectra were normalized to a frequency of 9.500 GHz. They were measured at RT with a microwave power of 200 mW, 8-mT sweep range, a recording time of 167 s, and a time constant of 0.3 s. The magnetic field was modulated at 10 kHz with an amplitude of 0.02 mT. Spectrum simulations were performed using the EasySpin libraries [REF-EASYSPIN] for MATLAB.

EPR spectra were recorded making use of the spin trap (DMPO). The samples were prepared according to the catalytic reaction mixture as follows: CTF-1-400 (17 mg), base (0.2 mmol), benzyl alcohol (34.3 μl, 0.33 mmol), and toluene (330 μl) were added to a vial open to air at RT. After around 5 min, DMPO (33 mg) was added to the reaction mixture. A screw-cap nuclear magnetic resonance tube was charged with 1 ml of the prepared reaction mixture and placed in the EPR cavity for the measurement. For the blank sample, the reaction

mixture was prepared similarly without the addition of CTF-1-400. Elemental analyses were performed on a Thermo Flash 200 elemental analyzer using V_2O_5 as catalyst.

SUPPLEMENTARY MATERIALS

Supplementary material for this article is available at http://advances.sciencemag.org/cgi/content/full/6/14/eaaz2310/DC1

REFERENCES AND NOTES

1. G. Stefanidis, A. Stankiewicz, *Alternative Energy Sources for Green Chemistry* (Royal Society of Chemistry, 2016).
2. D. Astruc, F. Lu, J. R. Aranzaes, Nanoparticles as recyclable catalysts: The frontier between homogeneous and heterogeneous catalysis. *Angew. Chem. Int. Ed. Engl.* **44**, 7852–7872 (2005).
3. J. M. Campelo, D. Luna, R. Luque, J. M. Marinas, A. A. Romero, Sustainable preparation of supported metal nanoparticles and their applications in catalysis. *ChemSusChem* **2**, 18–45 (2009).
4. M. V. Twigg, Homogeneous Catalysis of Organic Reactions by Transition Metal Complexes, in *Mechanisms of Inorganic and Organometallic Reactions* (Springer, 1991), pp. 339–367.
5. D. Halwidl, W. Mayr-Schmölzer, M. Setvin, D. Fobes, J. Peng, Z. Mao, M. Schmid, F. Mittendorfer, J. Redinger, U. Diebold, A full monolayer of superoxide: Oxygen activation on the unmodified $Ca_3 Ru_2 O_7$(001) surface. *J. Mater. Chem. A Mater.* **6**, 5703–5713 (2018).
6. X.-H. Li, J.-S. Chen, X. Wang, J. Sun, M. Antonietti, Metal-free activation of dioxygen by graphene/g-C3N4 nanocomposites: Functional dyads for selective oxidation of saturated hydrocarbons. *J. Am. Chem. Soc.* **133**, 8074–8077 (2011).
7. E. G. Kovaleva, J. D. Lipscomb, Crystal structures of Fe2+ dioxygenase superoxo, alkylperoxo, and bound product intermediates. *Science* **316**, 453–457 (2007).
8. T. H. Yosca, J. Rittle, C. M. Krest, E. L. Onderko, A. Silakov, J. C. Calixto, R. K. Behan, M. T. Green, Iron(IV)hydroxide pK(a) and the role of thiolate ligation in C-H bond activation by Cytochrome P450. *Science* **342**, 825–829 (2013).
9. Q. Fu, W.-X. Li, Y. Yao, H. Liu, H.-Y. Su, D. Ma, X.-K. Gu, L. Chen, Z. Wang, H. Zhang, B. Wang, X. Bao, Interface-confined ferrous centers for catalytic oxidation. *Science* **328**, 1141–1144 (2010).
10. S. F. Cai, H. Rong, X. Yu, X. Liu, D. Wang, W. He, Y. Li, Room temperature activation of oxygen by monodispersed metal nanoparticles: Oxidative dehydrogenative coupling of anilines for azobenzene syntheses. *ACS Catal.* **3**, 478–486 (2013).
11. M. M. Montemore, M. A. van Spronsen, R. J. Madix, C. M. Friend, O-2 activation by metal surfaces: Implications for bonding and reactivity on heterogeneous catalysts. *Chem. Rev.* **118**, 2816–2862 (2018).
12. X. Duan, K. O'Donnell, H. Sun, Y. Wang, S. Wang, Sulfur and nitrogen co-doped graphene for metal-free catalytic oxidation reactions. *Small* **11**, 3036–3044 (2015).
13. M. Liu, Z. Zhang, H. Liu, Z. Xie, Q. Mei, B. Han, Transformation of alcohols to esters promoted by hydrogen bonds using oxygen as the oxidant under metal-free conditions. *Sci. Adv.* **4**, eaas9319 (2018).
14. N. Kan-Nari, S. Okamura, S.-I. Fujita, J.-I. Ozaki, M. Arai, Nitrogen-doped carbon materials prepared by ammoxidation as solid base catalysts for knoevenagel condensation and transesterification reactions. *Adv. Synth. Catal.* **352**, 1476–1484 (2010).
15. Y. Cao, H. Yu, F. Peng, H. Wang, Selective allylic oxidation of cyclohexene catalyzed by nitrogen-doped carbon nanotubes. *ACS Catal.* **4**, 1617–1625 (2014).
16. A. Kumatani, C. Miura, H. Kuramochi, T. Ohto, M. Wakisaka, Y. Nagata, H. Ida, Y. Takahashi, K. Hu, S. Jeong, J.-I. Fujita, T. Matsue, Y. Ito, Chemical dopants on edge of holey graphene accelerate electrochemical hydrogen evolution reaction. *Adv. Sci.* **6**, 1900119 (2019).
17. L. Li, D. Cruz, A. Savateev, G. Zhang, M. Antonietti, Y. Zhao, Photocatalytic cyanation of carbon nitride scaffolds: Tuning band structure and enhancing the performance in green light driven C-S bond formation. *Appl. Catal. B Environ.* **229**, 249–253 (2018).
18. W. Wu, Q. Zhang, X. Wang, C. Han, X. Shao, Y. Wang, J. Liu, Z. Li, X. Lu, Enhancing selective photooxidation through co-nx-doped carbon materials as singlet oxygen photosensitizers. *ACS Catal.* **7**, 7267–7273 (2017).
19. L. Miao, D. Zhu, M. Liu, H. Duan, Z. Wang, Y. Lv, W. Xiong, Q. Zhu, L. Li, X. Chai, L. Gan, Cooking carbon with protic salt: Nitrogen and sulfur self-doped porous carbon nanosheets for supercapacitors. *Chem. Eng. J.* **347**, 233–242 (2018).
20. R. J. Gao, L. Pan, J. Lu, J. Xu, X. Zhang, L. Wang, J.-J. Zou, Phosphorus-doped and lattice-defective carbon as metal-like catalyst for the selective hydrogenation of nitroarenes. *ChemCatChem* **9**, 4287–4294 (2017).
21. S. Navalon, A. Dhakshinamoorthy, M. Alvaro, M. Antonietti, H. Garcia, Active sites on graphene-based materials as metal-free catalysts. *Chem. Soc. Rev.* **46**, 4501–4529 (2017).
22. W. Wei, H. Liang, K. Parvez, X. Zhuang, X. Feng, K. Müllen, Nitrogen-doped carbon nanosheets with size-defined mesopores as highly efficient metal-free catalyst for the oxygen reduction reaction. *Angew. Chem. Int. Ed.* **53**, 1570–1574 (2014).
23. S. Kawai, S. Nakatsuka, T. Hatakeyama, R. Pawlak, T. Meier, J. Tracey, E. Meyer, A. S. Foster, Multiple heteroatom substitution to graphene nanoribbon. *Sci. Adv.* **4**, eaar7181 (2018).
24. C. Rizescu, I. Podolean, J. Albero, V. I. Parvulescu, S. M. Coman, C. Bucur, M. Puche, H. Garcia, N-doped graphene as a metal-free catalyst for glucose oxidation to succinic acid. *Green Chem.* **19**, 1999–2005 (2017).
25. C. Tang, H.-F. Wang, X. Chen, B.-Q. Li, T.-Z. Hou, B. Zhang, Q. Zhang, M.-M. Titirici, F. Wei, Topological defects in metal-free nanocarbon for oxygen electrocatalysis. *Adv. Mater.* **28**, 6845–6851 (2016).
26. M. Latorre-Sánchez, A. Primo, H. García, P-doped graphene obtained by pyrolysis of modified alginate as a photocatalyst for hydrogen generation from water-methanol mixtures. *Angew. Chem. Int. Ed.* **52**, 11813–11816 (2013).
27. D. Liu, L. Wang, X. Feng, J. Liu, Y. Qin, Z. L. Wang, Chemical approaches to carbon-based metal-free catalysts. *Adv. Mater.* **31**, e1905436 (2019).
28. A. Dhakshinamoorthy, A. Primo, P. Concepcion, M. Alvaro, H. Garcia, Doped graphene as a metal-free carbocatalyst for the selective aerobic oxidation of benzylic hydrocarbons cyclooctane and styrene. *Chemistry* **19**, 7547–7554 (2013).
29. Y. Zhi, K. Li, H. Xia, M. Xue, Y. Mu, X. Liu, Robust porous organic polymers as efficient heterogeneous organo-photocatalysts for aerobic oxidation reactions. *J. Mater. Chem. A* **5**, 8697–8704 (2017).
30. H. Wang, Z. Zeng, P. Xu, L. Li, G. Zeng, R. Xiao, Z. Tang, D. Huang, L. Tang, C. Lai, D. Jiang, Y. Liu, H. Yi, L. Qin, S. Ye, X. Ren, W. Tang, Recent progress in covalent organic framework thin films: Fabrications, applications and perspectives. *Chem. Soc. Rev.* **48**, 488–516 (2019).
31. A. P. Côté, A. I. Benin, N. W. Ockwig, M. O'Keeffe, A. J. Matzger, O. M. Yaghi, Porous, crystalline, covalent organic frameworks. *Science* **310**, 1166–1170 (2005).
32. C. S. Diercks, O. M. Yaghi, The atom, the molecule, and the covalent organic framework. *Science* **355**, eaal1585 (2017).
33. P. Kuhn, M. Antonietti, A. Thomas, Porous, covalent triazine-based frameworks prepared by ionothermal synthesis. *Angew. Chem. Int. Ed. Engl.* **47**, 3450–3453 (2008).
34. M. Liu, L. Guo, S. Jin, B. Tan, Covalent triazine frameworks: Synthesis and applications. *J. Mater. Chem. A* **7**, 5153–5172 (2019).
35. S. Mukherjee, M. Das, A. Manna, R. Krishna, S. Das, Newly designed 1,2,3-triazole functionalized covalent triazine frameworks with exceptionally high uptake capacity for both CO_2 and H_2. *J. Mater. Chem. A* **7**, 1055–1068 (2019).
36. M. Liu, K. Jiang, X. Ding, S. Wang, C. Zhang, J. Liu, Z. Zhan, G. Cheng, B. Li, H. Chen, S. Jin, B. Tan, Controlling monomer feeding rate to achieve highly crystalline covalent triazine frameworks. *Adv. Mater.* **31**, e1807865 (2019).
37. K. Gontarczyk, W. Bury, J. Serwatowski, P. Wieciński, K. Woźniak, K. Durka, S. Luliński, Hybrid triazine-boron two-dimensional covalent organic frameworks: Synthesis, characterization, and DFT approach to layer interaction energies. *ACS Appl. Mater. Interfaces* **9**, 31129–31141 (2017).
38. C. B. Meier, R. S. Sprick, A. Monti, P. Guiglion, J.-S. M. Lee, M. A. Zwijnenburg, A. I. Cooper, Structure-property relationships for covalent triazine-based frameworks: The effect of spacer length on photocatalytic hydrogen evolution from water. *Polymer* **126**, 283–290 (2017).
39. S. Zhang, Q. Yang, C. Wang, X. Luo, J. Kim, Z. Wang, Y. Yamauchi, Porous organic frameworks: Advanced materials in analytical chemistry. *Adv. Sci.* **5**, 1801116 (2018).
40. P. Kuhn, A. Forget, D. Su, A. Thomas, M. Antonietti, From microporous regular frameworks to mesoporous materials with ultrahigh surface area: Dynamic reorganization of porous polymer networks. *J. Am. Chem. Soc.* **130**, 13333–13337 (2008).
41. X. Hu, Y. Long, M. Fan, M. Yuan, H. Zhao, J. Ma, Z. Dong, Two-dimensional covalent organic frameworks as self-template derived nitrogen-doped carbon nanosheets for eco-friendly metal-free catalysis. *Appl. Catal. B Environ.* **244**, 25–35 (2019).
42. S. Hug, L. Stegbauer, H. Oh, M. Hirscher, B. V. Lotsch, Nitrogen-rich covalent triazine frameworks as high-performance platforms for selective carbon capture and storage. *Chem. Mater.* **27**, 8001–8010 (2015).
43. O. Buyukcakir, S. H. Je, S. N. Talapaneni, D. Kim, A. Coskun, Charged covalent triazine frameworks for CO_2 capture and conversion. *ACS Appl. Mater. Interfaces* **9**, 7209–7216 (2017).
44. D. Y. Osadchii, A. I. Olivos-Suarez, A. V. Bavykina, J. Gascon, Revisiting nitrogen species in covalent triazine frameworks. *Langmuir* **33**, 14278–14285 (2017).
45. L. Hao, B. Luo, X. Li, M. Jin, Y. Fang, Z. Tang, Y. Jia, M. Liang, A. Thomas, J. Yang, L. Zhi, Terephthalonitrile-derived nitrogen-rich networks for high performance supercapacitors. *Energ. Environ. Sci.* **5**, 9747–9751 (2012).
46. K. S. Walton, R. Q. Snurr, Applicability of the BET method for determining surface areas of microporous metal-organic frameworks. *J. Am. Chem. Soc.* **129**, 8552–8556 (2007).
47. L. Hao, J. Ning, B. Luo, B. Wang, Y. Zhang, Z. Tang, J. Yang, A. Thomas, L. Zhi, Structural evolution of 2D microporous covalent triazine-based framework toward the study of high-performance supercapacitors. *J. Am. Chem. Soc.* **137**, 219–225 (2015).

48. H. Watanabe, S. Asano, S.-i. Fujita, H. Yoshida, M. Arai, Nitrogen-doped, metal-free activated carbon catalysts for aerobic oxidation of alcohols. *ACS Catal.* **5**, 2886–2894 (2015).
49. M. A. Patel, F. Luo, M. R. Khoshi, E. Rabie, Q. Zhang, C. R. Flach, R. Mendelsohn, E. Garfunkel, M. Szostak, H. He, P-doped porous carbon as metal free catalysts for selective aerobic oxidation with an unexpected mechanism. *ACS Nano* **10**, 2305–2315 (2016).
50. J. L. Long, X. Xie, J. Xu, Q. Gu, L. Chen, X. Wang, Nitrogen-doped graphene nanosheets as metal-free catalysts for aerobic selective oxidation of benzylic alcohols. *Acs Catal.* **2**, 622–631 (2012).
51. K. W. Wang, L. M. Yang, X. Wang, L. Guo, G. Cheng, C. Zhang, S. Jin, B. Tan, A. Cooper, Covalent triazine frameworks via a low-temperature polycondensation approach. *Angew Chem Int Ed. Engl.* **56**, 14149–14153 (2017).
52. R. Pietrzak, H. Wachowska, P. Nowicki, Preparation of nitrogen-enriched activated carbons from brown coal. *Energy Fuels* **20**, 1275–1280 (2006).
53. J. Jia, Z. Chen, Y. Belmabkhout, K. Adil, P. M. Bhatt, V. A. Solovyeva, O. Shekhah, M. Eddaoudi, Carbonization of covalent triazine-based frameworks via ionic liquid induction. *J. Mater. Chem. A* **6**, 15564–15568 (2018).
54. W. Huang, B. C. Ma, H. Lu, R. Li, L. Wang, K. Landfester, K. A. I. Zhang, Visible-light-promoted selective oxidation of alcohols using a covalent triazine framework. *ACS Catal.* **7**, 5438–5442 (2017).
55. W. Spiller *et al.*, Singlet oxygen quantum yields of different photosensitizers in polar solvents and micellar solutions. *J. Porphyr. Phthalocyanines* **2**, 145–158 (1998).
56. G. R. Buettner, Spin trapping: ESR parameters of spin adducts 1474 1528V. *Free Radic. Biol. Med.* **3**, 259–303 (1987).
57. M. Lee, S. B. Chang, Highly efficient aerobic oxidation of benzylic and allylic alcohols by a simple catalyst system of $[RuCl_2(p\text{-cymene})]_2/Cs_2CO_3$. *Tetrahedron Lett.* **41**, 7507–7510 (2000).
58. R. M. Sellers, Spectrophotometric determination of hydrogen peroxide using potassium titanium(Iv) oxalate. *Analyst* **105**, 950–954 (1980).
59. X. Hu, Y. Wu, H. Li, Z. Zhang, Adsorption and activation of O_2 on nitrogen-doped carbon nanotubes. *J. Phys. Chem. C* **114**, 9603–9607 (2010).
60. D. Eisenberg, T. K. Slot, G. Rothenberg, Understanding oxygen activation on metal- and nitrogen-codoped carbon catalysts. *ACS Catal.* **8**, 8618–8629 (2018).
61. J. Di, J. Xia, X. Chen, M. Ji, S. Yin, Q. Zhang, H. Li, Tunable oxygen activation induced by oxygen defects in nitrogen doped carbon quantum dots for sustainable boosting photocatalysis. *Carbon* **114**, 601–607 (2017).
62. Z. Li, W. Zhao, C. Yin, L. Wei, W. Wu, Z. Hu, M. Wu, Synergistic effects between doped nitrogen and phosphorus in metal-free cathode for zinc-air battery from covalent organic frameworks coated CNT. *ACS Appl. Mater. Interfaces* **9**, 44519–44528 (2017).
63. A. E. Wendlandt, S. S. Stahl, Chemoselective organocatalytic aerobic oxidation of primary amines to secondary imines. *Org. Lett.* **14**, 2850–2853 (2012).
64. C. Su, M. Acik, K. Takai, J. Lu, S.-J. Hao, Y. Zheng, P. Wu, Q. Bao, T. Enoki, Y. J. Chabal, K. P. Loh, Probing the catalytic activity of porous graphene oxide and the origin of this behaviour. *Nat. Commun.* **3**, 1298 (2012).
65. S. Abednatanzi, P. G. Derakhshandeh, A. Abbasi, P. Van Der Voort, K. Leus, Direct synthesis of an iridium(III) bipyridine metal–organic framework as a heterogeneous catalyst for aerobic alcohol oxidation. *ChemCatChem* **8**, 3672–3679 (2016).
66. S. Abednatanzi, K. Leus, P. G. Derakhshandeh, F. Nahra, K. De Keukeleere, K. Van Hecke, I. Van Driessche, A. Abbasi, S. P. Nolan, P. Van Der Voort, POM@IL-MOFs–inclusion of POMs in ionic liquid modified MOFs to produce recyclable oxidation catalysts. *Cat. Sci. Technol.* **7**, 1478–1487 (2017).

Acknowledgments: We are grateful to J. Goeman for experimental help with the GC–mass spectrometry analyses. We thank K. Haustraete for the STEM measurements. **Funding:** This work was financially supported by Ghent University BOF doctoral grant 01D04318 and the Research Foundation Flanders (FWO-Vlaanderen) grant no. G000117N. **Author contributions:** P.V.D.V. conceived the project. S.A., P.G.D., K.L., and A.S. synthesized the catalysts and performed the characterization and catalytic experiments. J.S. conceived and performed the XPS experiments. H.V. and F.C. conceived and performed the EPR experiments. All authors interpreted the data and contributed to preparation of the manuscript. **Competing interests:** The authors declare that they have no competing interests. **Data and materials availability:** All data needed to evaluate the conclusions in the paper are present in the paper and/or the Supplementary Materials. Additional data related to this paper may be requested from the authors.

Submitted 23 August 2019
Accepted 9 January 2020
Published 3 April 2020
10.1126/sciadv.aaz2310

Citation: S. Abednatanzi, P. Gohari Derakhshandeh, K. Leus, H. Vrielinck, F. Callens, J. Schmidt, A. Savateev, P. Van Der Voort, Metal-free activation of molecular oxygen by covalent triazine frameworks for selective aerobic oxidation. *Sci. Adv.* **6**, eaaz2310 (2020).

Science Advances

Metal-free activation of molecular oxygen by covalent triazine frameworks for selective aerobic oxidation

Sara Abednatanzi, Parviz Gohari Derakhshandeh, Karen Leus, Henk Vrielinck, Freddy Callens, Johannes Schmidt, Aleksandr Savateev and Pascal Van Der Voort

Sci Adv **6** (14), eaaz2310.
DOI: 10.1126/sciadv.aaz2310